JOINT INSTITUTE FOR NUCLEAR RESEARCH

Dzhelepov laboratory of Nuclear Problems

FINAL REPORT ON THE START PROGRAMME

Study of light collection function in JUNO detector

Supervisor:
Dr. Oleg Yurievich Smirnov

Student:
Kirill Kiselev, Russia
National Research Nuclear
University "MEPHI"

Participation period:
June 30 – August 10,
Summer Session 2024

Dubna, 2024

ABSTRACT

Generating events in large scintillator detectors like JUNO by tracking the path of each scintillation photon from emission to capture is a slow process. Additionally, the generated data may not match the real data collected by the detector. To address these issues, we propose an analytical approximation of the detector response based on the relative positions of the generated event and the PMTs in the detector. In this study, we establish the parameters of the model and extract them from the data generated for the JUNO detector.

CONTENTS

INTRODUCTION

THE JUNO DETECTOR

JUNO (Jiangmen Underground Neutrino Observatory) is a large underground liquid scintillator detector located in an underground laboratory under the Dashi hill (700 m underground) in Jinji town in Guangdong province, China [1]. The primary physics goal of the JUNO detector was proposed to be the determination of the neutrino mass ordering [2], however other neutrino oscillation and astroparticle physics topics will be researched.

The Central Detector (CD) of JUNO will be a spherical acrylic vessel 35.4 m in inner diameter and 120 mm thick containing 20 kton LAB-based (linear alkylbenzene) liquid scintillator and supported by a spherical stainless steel (SS) structure (see fig. 1). The CD volume will be watched by 17612 20-inch "large" PMTs (photomultiplier tubes) and 25600 3-inch "small" PMTs. The cylindrical Water Pool (WP), in which the CD will be contained, will be filled with 35 ktons of ultrapure water and will be watched by 2400 20-inch PMTs to create a Cherenkov detector for vetoing muons. Also a part of the veto, the Top Tracker (TT) will be located above the main detector and will consist of plastic scintillating strips.

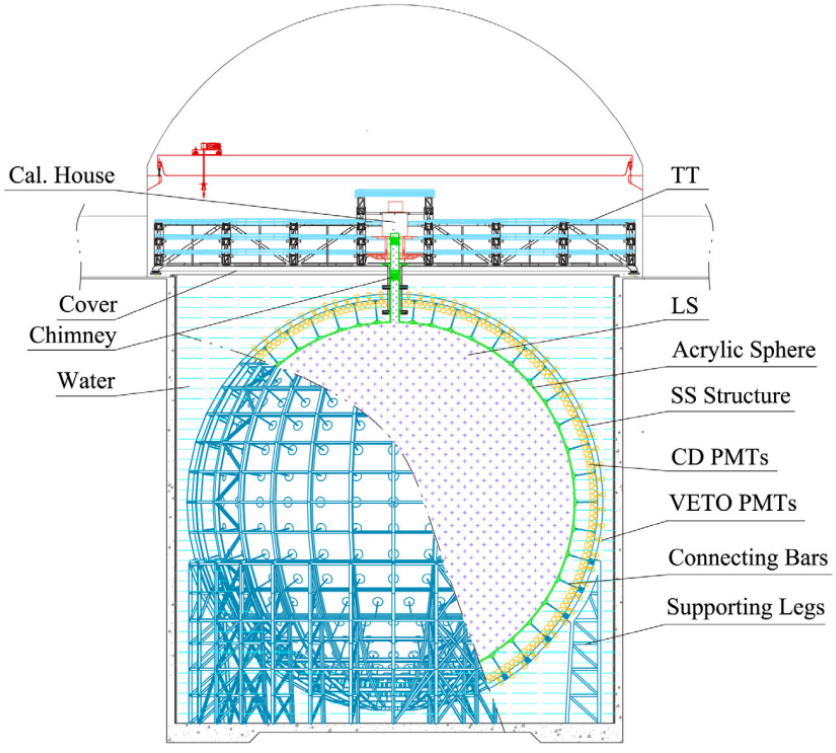

Fig. 1 — Schematic view of the JUNO detector [1]

DETECTOR RESPONSE MODELING

Usually the response of a detector is modelled using toolkits such as Geant4, which allow to simulate the geometry of the detector, its materials and the passage of particles through it. Such methods are used ubiquitously: in high energy, nuclear and neutrino physics, medical science, etc. It allows for detailed event generation, e.g. in a given scintillation event the path of each photon through matter is tracked from its emission to its capture in the detector and then the response of detector electronics is also simulated. This way of modeling, while being very thorough and giving large amounts of data for preliminary and ongoing study of the detector, can be quite slow, taking seconds to generate a single event, while in a real detector event frequency may easily measure in thousands per second.

A more «phenomenological» path of event generation was used in the CTF experiment [3; 4] and discussed in [5]: it consists of defining an analytical approximation of the detector response with some free parameters, evaluating their values from fitting the approximation to real or generated data and then generating events based on the approximation. Here a similar (albeit simplified) analysis is reported for the generated data of the JUNO detector.

1 PHOTOMULTIPLIER TUBES

1.1 CD LPMT COORDINATES AND TYPES

In this analysis, we only consider the "large" (20-inch) PMTs (or LPMTs) of the CD. The coordinates of these PMTs will be needed.

There are two types of LPMTs in the CD: Microchannel Plate Photomultipliers (MCP PMTs) and dynode PMTs. The MCP PMTs from Northern Night Vision Technology Co. are further divided into two categories: NNVT (2720 PMTs) and HighQENNVT (9825 PMTs). Dynode PMTs from Hamamatsu Photonics K. number 4997 PMTs. In this analysis, we divided the PMTs into these three types. In JUNO software, each of the LPMTs of the CD is given an ID from 0 to 17611, and the coordinates and type of each PMT are also known (see fig. 1.1). The distance between each PMT and the center of the detector is $L_0 = 19.4$ m.

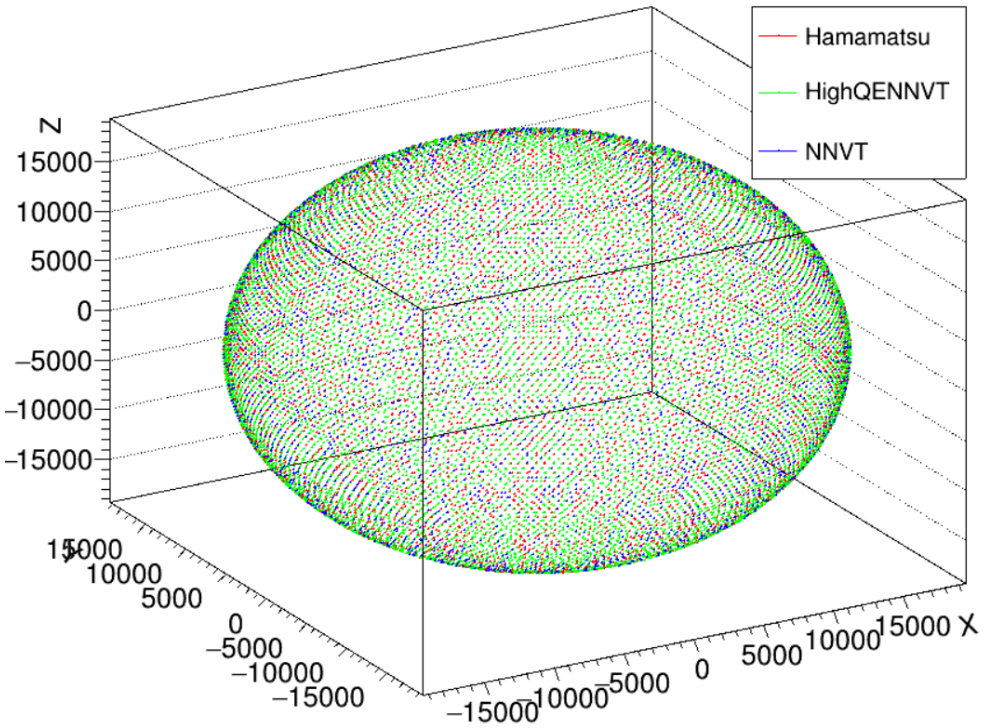

Fig. 1.1 — The arrangement of PMTs in JUNO CD by type: Hamamatsu (red), HighQENNVT (green) and NNVT (blue). The coordinates are measured in mm.

To determine what the coordinates of a given PMT represent in the frame of reference of the PMT, a few electronic events were generated at the center of the CD and the

positions where the scintillation photons hit the PMT surface were displayed along with the coordinates of the PMT itself (see fig 1.2). As can be seen from the figure, the PMT coordinates give the position of the geometric center of the PMT photocathode surface (a point «inside» it). In our analysis, however, we used the coordinates of the «top» of the photocathode surface. These can be calculated if the distance between the two points for each PMT type is known: ∼190 mm for Hamamatsu and ∼184 mm for NNVT.

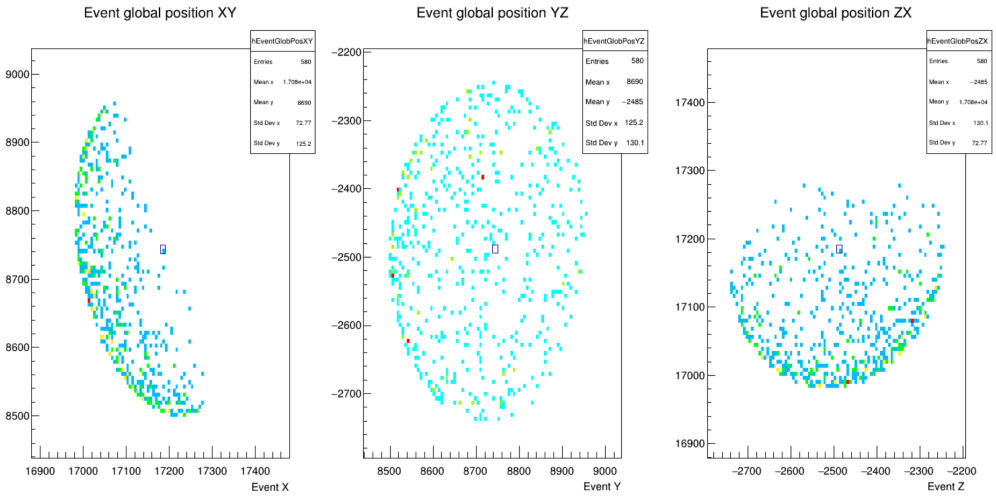

Fig. 1.2 — Three projections of the points where scintillation photons hit the PMT surface (the color of bins marks the number of hits in each bin) and the PMT coordinates (box). The coordinates are measured in mm.

1.2 CD LPMT SENSITIVITIES

Each of the LPMTs of the CD of JUNO responds somewhat differently to the scintillation photons hitting its photocathode and the photo electrons (p.e.) emitted from it — the average collected charge will not be the same for all the PMTs. Owing to spherical symmetry of the JUNO CD, we normalized all values to the center of the detector. First, we must calculate the average charge $\langle Q_0 \rangle$ (in p.e.) collected per event located in the center of the detector and divide it by the number of PMTs [5]:

$$\mu_0 = \frac{\langle Q_0 \rangle}{N_{PMT}} \tag{1.1}$$

As there are 17612 LPMTs in the CD and the expected yield of photons in a scintillation event is $\sim 1600 \frac{\text{p.e.}}{\text{MeV}}$ [1], the value of μ_0 is $\approx 0.1 \frac{\text{p.e.}}{\text{MeV}\cdot\text{event}\cdot\text{PMT}}$.

To extract μ_0, $N_{ev} = 10^5$ events of a 1 MeV single electron at the center of the detector were generated, and the response of the LPMTs was analyzed. From the obtained data files, two branches were taken for analysis: «Charge», a branch with a data type double, and «nPE_perPMT» (number of p.e.) with a data type integer. The values of μ_0 were calculated for all PMTs together and then for the three PMT types separately (Tab. 1.1). As shown in the table, the different PMT types have distinctly different values of μ_0.

Moreover, to correctly calculate the error of each μ_0 value, we must account for the variance of signal multiplication in PMTs due to its statistical nature. Each photoelectron, multiplied by the PMT dynode system, creates a slightly different signal in the outer circuit. This results in an increase in the variance of the output signals relative to the input signals. The factor by which the variance increases is called the excess noise factor (ENF), which has been measured for the PMTs of the JUNO detector [6]. The measured ENF is 1.19 for Hamamatsu PMTs and 1.58 for NNVT PMTs (see fig. 1.3).

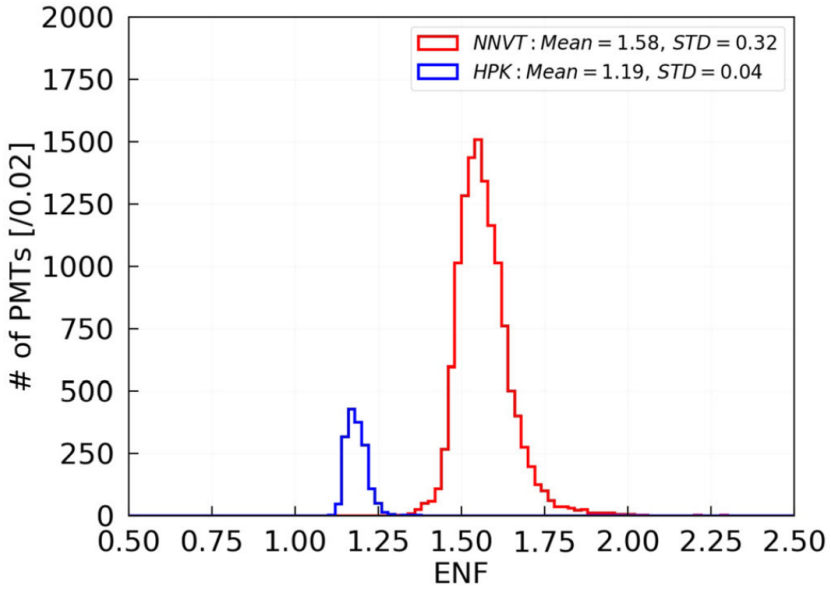

Fig. 1.3 — Excess noise factor (ENF) distribution for the PMTs of the JUNO detector [6]

The distribution of the number of photoelectrons follows Poisson's law; therefore, the error of μ_0 values can be calculated as follows:

$$\Delta\mu_0 = \Delta\left(\frac{\langle Q_0\rangle}{N_{PMT}}\right) = \frac{\Delta\langle Q_0\rangle}{N_{PMT}} = \frac{1}{N_{PMT}}\sqrt{\frac{\mathrm{ENF}\cdot\langle Q_0\rangle}{N_{ev}}} \tag{1.2}$$

Another way of interpreting μ_0 is to consider it as the mean value of the Poisson distribution of the number of p.e. that are emitted from the surface of a single PMT in an event. Given this, its value can also be extracted from the number N of PMTs that registered at least one p.e. This branch of analysis is called «N PMT».

The probability of 0 p.e. emission is $P(0) = e^{-\mu_0}$. Then, a nonzero amount of p.e. is emitted with a probability of $P(>0) = 1 - P(0) = 1 - e^{-\mu_0}$. Experimentally, $P(>0)$ can be determined as the ratio of N to $N_{trig} = N_{ev}\cdot N_{PMT}$ — the total number of triggers (the number of times a PMT could have registered a signal). Thus, μ_0 can be calculated as

$$\mu_0 = -\ln\left(1 - \frac{N}{N_{trig}}\right) \tag{1.3}$$

The value N follows a binomial distribution with $p = P(>0)$ («success» — PMT

registered a signal) and $q = 1 - P(> 0) = P(0)$ («failure» — PMT has not registered anything). From the dispersion of this binomial distribution $D[N] = N_{trig}pq$, we can evaluate the error of the μ_0 value as:

$$\Delta\mu_0 = \Delta\left(-\ln\left(1 - \frac{N}{N_{trig}}\right)\right) = \frac{N_{trig}}{N_{trig} - N}\frac{\Delta N}{N_{trig}} = \sqrt{\frac{N}{N_{trig}(N_{trig} - N)}} \tag{1.4}$$

Branch	Average μ_0	μ_0 by PMT type		
		Hamamatsu	HighQENNVT	NNVT
Charge	0.10617±0.00001	0.08621±0.00001	0.11495±0.00001	0.11094±0.00001
nPE_perPMT	0.11819±0.00001	0.10015±0.00002	0.12627±0.00001	0.12194±0.00003
N PMT	0.10337±0.00001	0.09226±0.00001	0.10862±0.00001	0.10481±0.00002

Table 1.1 — The average charge μ_0 per event (1 MeV electron in the center of the detector) per PMT for different branches of the analysis and different PMT types

Using the acquired values of μ_0 we can extract the sensitivities s_i of each PMT. Using the same generated data sample, we calculate the average charge μ_i collected by the i-th PMT per event and divide it by the respective μ_0 [5]:

$$s_i = \frac{\mu_i}{\mu_0} \tag{1.5}$$

The value of μ_i can be calculated either by taking the ratio of the charge Q_i collected by the i-th PMT to the number of events N_{ev} or by taking the mean value of the Poisson distribution of the p.e. counts in each event, in which case the number of triggers is $N_{trig} = N_{ev}$, because the calculation is performed for each PMT separately. The errors of s_i can also be calculated as:

$$\Delta s_i = \sqrt{\left(\frac{\Delta\mu_i}{\mu_0}\right)^2 + \left(\frac{\mu_i\Delta\mu_0}{\mu_0^2}\right)^2} \tag{1.6}$$

where $\Delta\mu_0$ is the error in μ_0 (Eq. 1.2, 1.4) and the errors $\Delta\mu_i$ are calculated the same way.

When the calculation of s_i is performed using the average values for μ_0, the distinction between the sensitivities of different PMT types is easily visible (compare fig. 1.4 and 1.5).

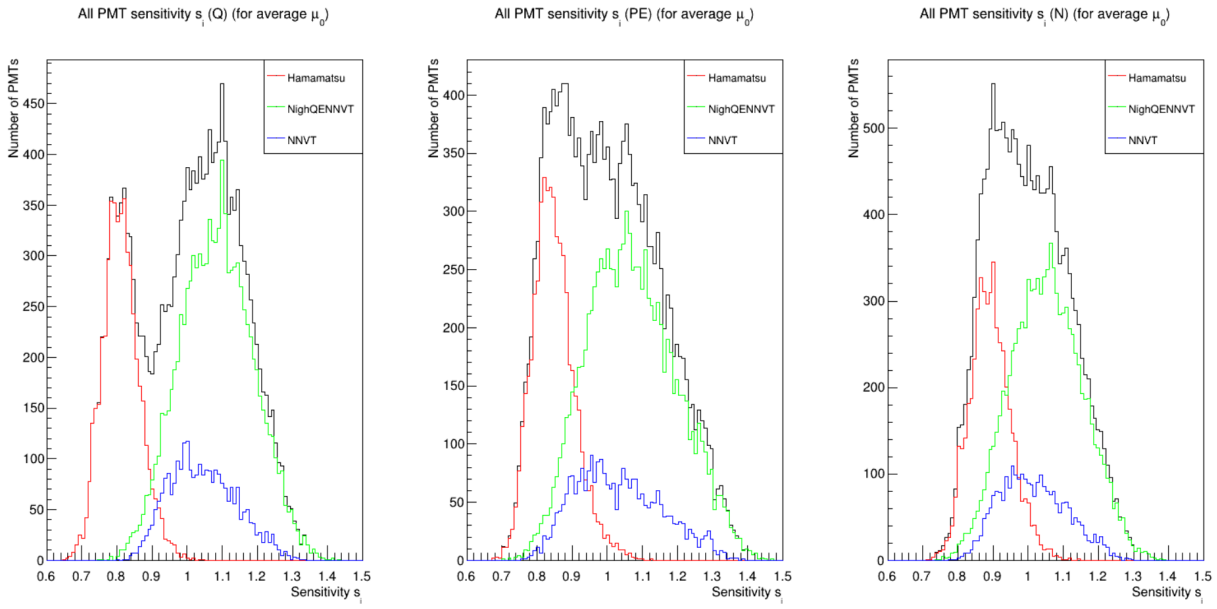

Fig. 1.4 — PMT sensitivities s_i calculated using the average μ_0 values for the respective branches: «Charge» (left), «nPE_perPMT» (center) and «N PMT» (right)

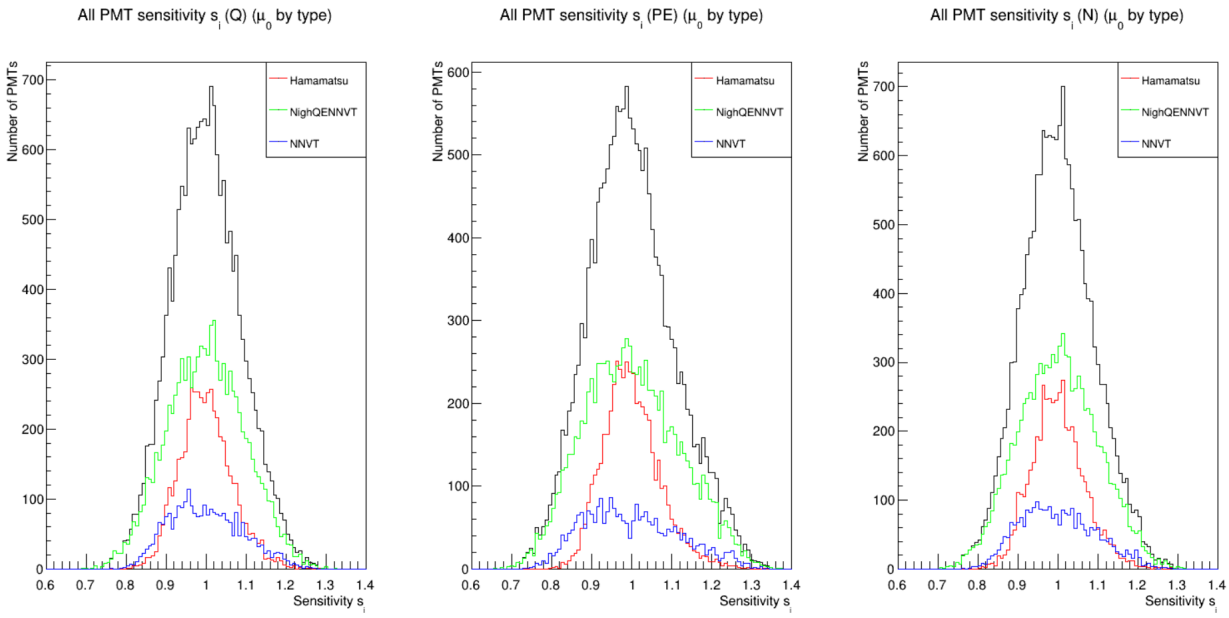

Fig. 1.5 — PMT sensitivities s_i calculated using μ_0 values corresponding to each PMT type for the respective branches: «Charge» (left), «nPE_perPMT» (center) and «N PMT» (right)

2 PMT LIGHT COLLECTION FUNCTION

Previously, all analysis was conducted for events generated in the center of the detector. However, it is only logical that events closer to a given PMT will produce a greater output signal, whereas farther ones may not even be registered. This effect can be considered by introducing a factor that depends on the event position relative to the PMT. We call this factor the **PMT light collection function** f_{PMT}.

2.1 GEOMETRY

The position of each event can be described using the coordinates $\mathbf{r} = \{x, y, z\}$ (in the detector frame of reference) or the coordinates in the frame of reference of the i-th PMT: the distance L_i between the PMT and event and the polar angle θ_i' at which the PMT «sees» the event. We assume axial symmetry of the photocathode sensitivity, thus we do not need a third coordinate (the azimuthal angle) for the PMT frame of reference. Another pair of coordinates can be introduced to describe the event position: the distance from the center of the detector $r = \sqrt{x^2 + y^2 + z^2}$ (which is the same for all the PMTs) and the angle θ_i between $\mathbf{r}$ and $\mathbf{R}_i$ (the position of the i-th PMT in the detector frame of reference).

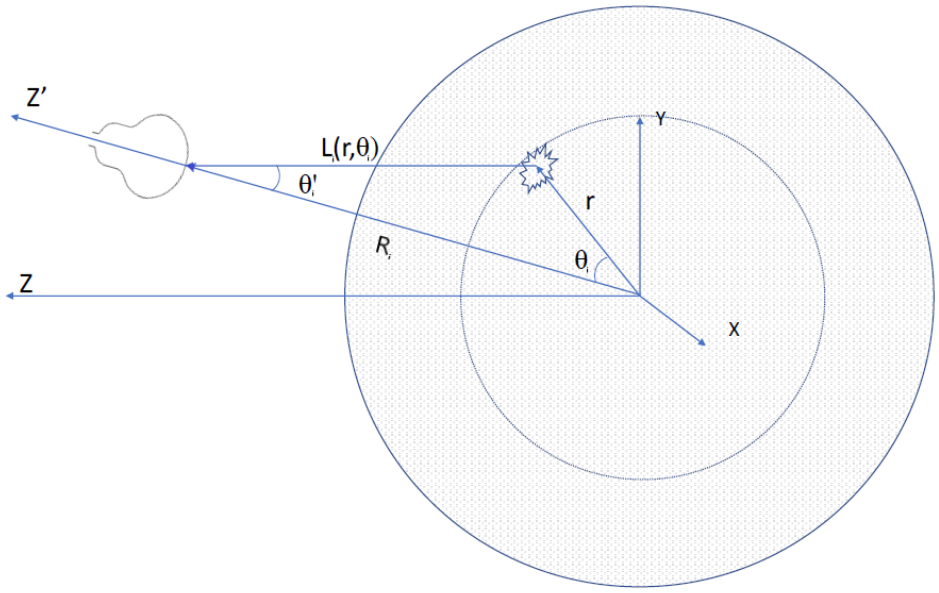

Fig. 2.1 — Positions of a PMT, of an event, and the coordinates used to describe them: $\{r, \cos\theta_i\}$ and $\{L_i, \cos\theta_i'\}$. The shaded volume shows the CD filled with scintillator: a sphere with the radius of $R = 17.7$ m [5]

All the coordinate transformations can be easily drawn from geometry (Fig. 2.1):

$$\cos\theta_i = \frac{\mathbf{R}_i \cdot \mathbf{r}}{R_i\, r} \tag{2.1}$$

$$L_i(r, \cos\theta_i) = \sqrt{r^2 + R_i^2 - 2rR_i\cos\theta_i} \tag{2.2}$$

$$\cos\theta_i'(r, \cos\theta_i) = \frac{R_i - r\cos\theta_i}{L_i(r, \theta_i)} \tag{2.3}$$

2.2 EXTRACTING THE PMT LIGHT COLLECTION FUNCTION

Let us define the PMT light collection function $f_{PMT}(r, \cos\theta_i)$ as the factor that relates the average charge μ_i collected by the i-th PMT for an event in the center of the detector to the average charge $\mu_i(r, \cos\theta_i)$ collected by the same PMT for an event with coordinates $\{r, \cos\theta_i\}$:

$$\mu_i(r, \cos\theta_i) = \mu_i \cdot f_{PMT}(r, \cos\theta_i) = \mu_0 \cdot s_i \cdot f_{PMT}(r, \cos\theta_i) \tag{2.4}$$

To determine the PMT light collection function, we first must to generate events evenly distributed in the volume of the detector. We allocate events into the cells of an $r \times \cos\theta_i$ histogram, and all cells must contain an equal volume (≈ 1 m^3) of the liquid scintillator to ensure that the events are evenly distributed between them. Thus, the cell boundaries must be equidistant on a grid of $r^3 \times \cos\theta_i = [0; 17^3]$ m^3 $\times$ $[-1; 1]$.

To obtain sufficient statistics (at least $\approx 10^4$ events per cell) for each PMT type, 400000 events of a 1 MeV single electron were generated in the volume of the detector. The «Charge» and «nPE_perPMT» branches were put into respective histograms (after dividing them by μ_0 and s_i), and an additional histogram was created to record the number of PMTs that collected a non-zero charge for an alternative charge calculation (see eq. 1.3).

To correctly normalize the histograms, we must record not only the charge collected in each cell but also the number of triggers in each cell. This means that with each generated event, we must record a trigger for each PMT (increase the number of entries in the cell of a «trigger» histogram by 1), regardless of whether or not the PMT has «seen» the event. We accounted for the pseudo-random nature of the generation of events distributed uniformly in the detector volume by dividing the charge by the number of triggers in each cell.

As a result, each cell of the «Charge» and «nPE_perPMT» histograms contains the value

$$\frac{Q}{\mu_0 N_{tr}} = \frac{\sum_{k=0}^{N_{ev}} \sum_{i=0}^{N_{PMT}} \frac{\mu_i^{(k)}}{s_i \mu_0}}{\sum_{k=0}^{N_{ev}} \sum_{i=0}^{N_{PMT}} 1} \tag{2.5}$$

where Q is the total charge (p.e.) collected in the cell, N_{tr} is the number of triggers in the cell, $\mu_i^{(k)}$ is the charge (p.e.) collected in the k-th event by the i-th PMT (which can be 0 if a PMT did not register an event), s_i is the sensitivity of the i-th PMT, N_{PMT} is the number of PMTs of a given type, N_{ev} is the number of generated events.

Each cell of the «N PMT» histogram contains the value

$$-\ln\left(1 - \frac{N}{N_{tr}}\right) = -\ln\left(1 - \frac{\sum_{k=0}^{N_{ev}} \sum_{i=0}^{N_{PMT}} \frac{1}{s_i} \cdot \mathrm{H}(\mu_i^{(k)})}{\sum_{k=0}^{N_{ev}} \sum_{i=0}^{N_{PMT}} 1}\right) \tag{2.6}$$

Here N is the total number of PMTs that have collected a non-zero charge, H(x) is the Heaviside step function.

The errors for each cell of the «Charge» and «nPE_perPMT» histograms are then calculated as follows:

$$\Delta\left(\frac{Q}{N_{tr}}\right) = \frac{\sqrt{Q \cdot \mathrm{ENF}}}{N_{tr}} \tag{2.7}$$

The errors of the «N PMT» histogram are calculated using Eq. 1.4.

2.3 FITTING THE PMT LIGHT COLLECTION FUNCTION

An analytical approximation for the PMT light collection function was used to fit the histograms [5]:

$$f_{PMT}(r, \cos\theta) = f_0 \cdot \left(\frac{L(r, \cos\theta)}{L_0}\right)^m \cdot \cos^n \theta'(r, \cos\theta) \cdot \exp\left(-\frac{L(r, \cos\theta) - L_0}{L_{att}}\right) + D \tag{2.8}$$

Here, r and $\cos\theta$ are the coordinates of an event relative to the PMT (Fig. 2.1), f_0 is the normalizing parameter (in order of ≈ 1), $L(r, \cos\theta)$ and $\cos^n \theta'(r, \cos\theta)$ are defined in 2.1-2.3, m is a parameter that is either fixed at $m = 2$ (accounts for the solid angle, the light propagation is considered to be isotropic) or is close to 2 (for a slightly better fit), n is a parameter of the fitting function that describes the angular dependancy, L_{att} is the parameter representing the attenuation length in the liquid scintillator (in order of ≈ 20 m [7]) and D is the constant that accounts for the dark noise of the PMTs. Note that without the dark noise of PMTs ($D = 0$) and with f_0 set to 1, the PMT light collection function is

equal to 1 at the center of the detector.

To estimate the dark noise constant D and fit the histograms we require the trigger window for each event $T_{tr} = 300$ ns and the dark rate of each PMT $\nu_{DR} = 30000\ s^{-1}$, which is the same for every PMT type. The distribution of dark pulses in a PMT follows a Poisson distribution, with a mean of $\mu = T_{tr}\,\nu_{DR} = 0.009 \frac{\text{dark p.e.}}{\text{PMT}\cdot\text{event}}$. To fit each histogram, we must divide this value by the respective μ_0: $D = \frac{0.009}{\mu_0}$.

The fitting of the «Charge» and «N PMT» histograms was performed. One result of a fit (for the Hamamatsu PMT type and «Charge» branch of analysis) is shown in Figure 2.2.

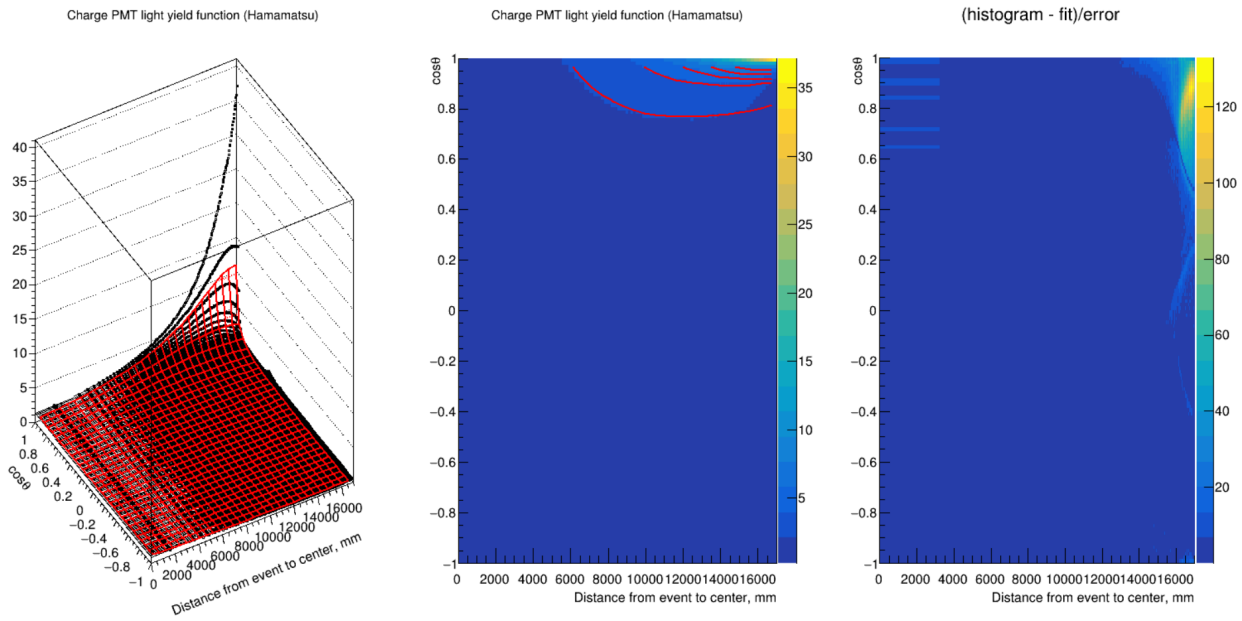

Fig. 2.2 — Histogram and the function (red) used to fit it. 3D view (left), 2D view (center) and the residuum histogram (in each bin the difference between the histogram value and fitting function is divided by the error of the same bin)

At high values of f_{PMT} the number of PMTs («N PMT» branch) badly represents the charge collected (and, consequently, the particle energy); if an event happens very near a PMT, it will likely collect multiple p.e. of charge; however, that would still only count as one PMT in Eq. 2.6 as the step function H(x) can either be equal to 0 or to 1. This implies that we must to restrict our region of fitting to the area where $f_{PMT} \cdot \mu_0 \ll 1$ or $f_{PMT} < 1$. Such restrictions were applied to the fit (for example, Fig. 2.3).

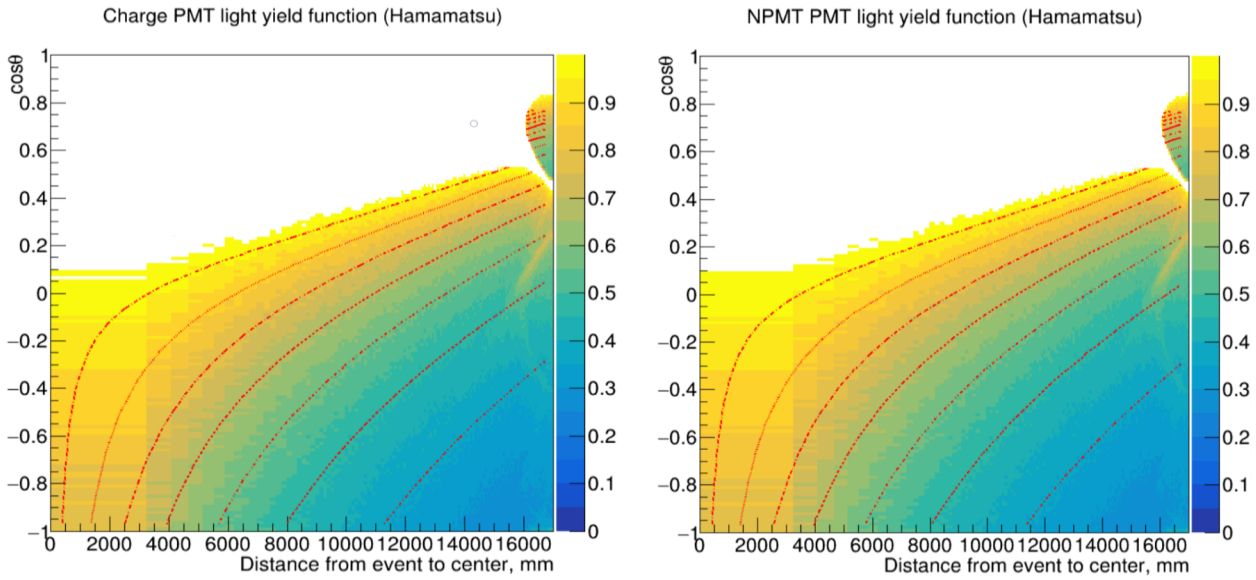

Fig. 2.3 — Histograms «Charge» (left) and «N PMT» (right) for Hamamatsu PMT, fitted in the region, where the bin contents don't exceed 1

The zone that stands out significantly in the fit is the marginal zone near the PMT: $r \lesssim R$, $\cos\theta \in (0.5; 0.9)$. This zone forms because of the total internal reflection at the boundary between the liquid scintillator (refractive index $n_{LS} \approx \frac{3}{2}$ [8]) and water (refractive index $n_{H_2O} \approx \frac{4}{3}$), as shown in Appendix A.

To determine the «best» radial region of fit, a series of fits with varied higher radial limits was conducted for the «Charge» and «N PMT» branches and for each of the PMT types. The results of the fit (reduced χ^2 and parameters of the analytical approximation) are displayed in fig. 2.4 and 2.5. The «best» fit corresponds to a higher radial limit $\approx \frac{R}{2}$.

The results are inconsistent across PMT types: the values of L_{att} are very different. The closest to the expected value is the result of the Hamamatsu PMT with a non-fixed parameter m: the parameter values span $L_{att} \in (20.1; 23.9)$ m.

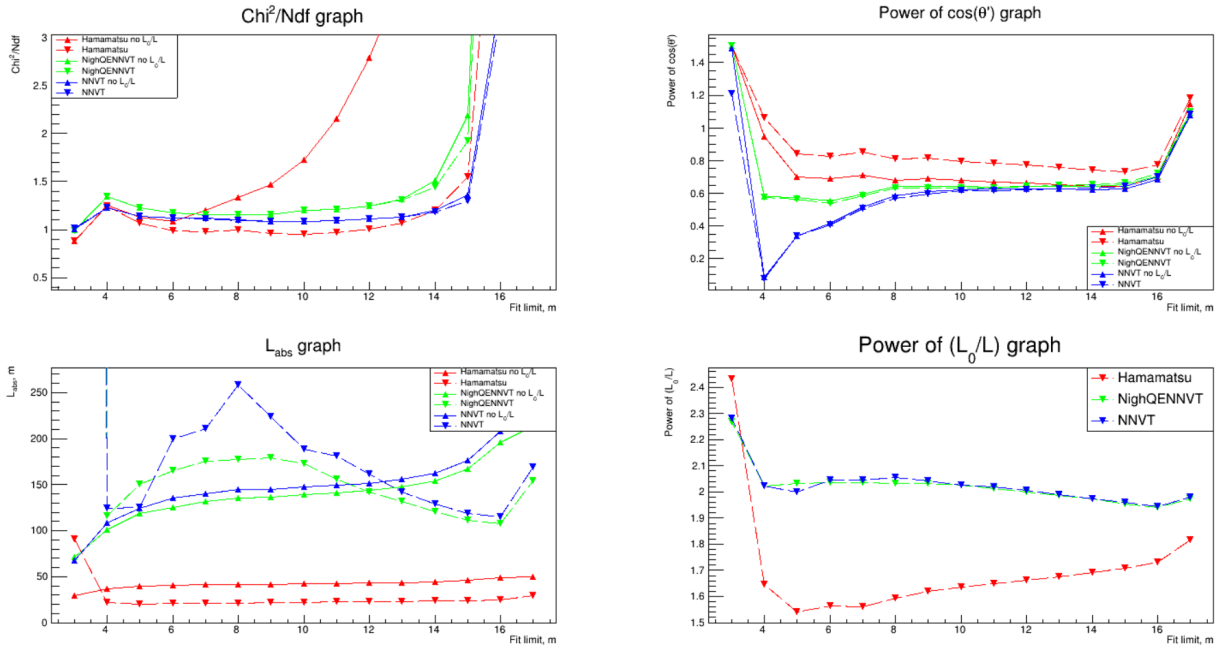

Fig. 2.4 — The results of the «Charge» histogram fit by the analytical function (see Eq. 2.8) for each PMT type: Hamamatsu (red), HighQENNVT (green) and NNVT (blue). The graphs include the reduced χ^2 (upper right) and parameters of the fit: n (upper left), L_{att} (lower left) and m (lower right). If the parameter m of the fit is fixed at $m = 2$, the line is solid, if m is not fixed, then the line is dashed

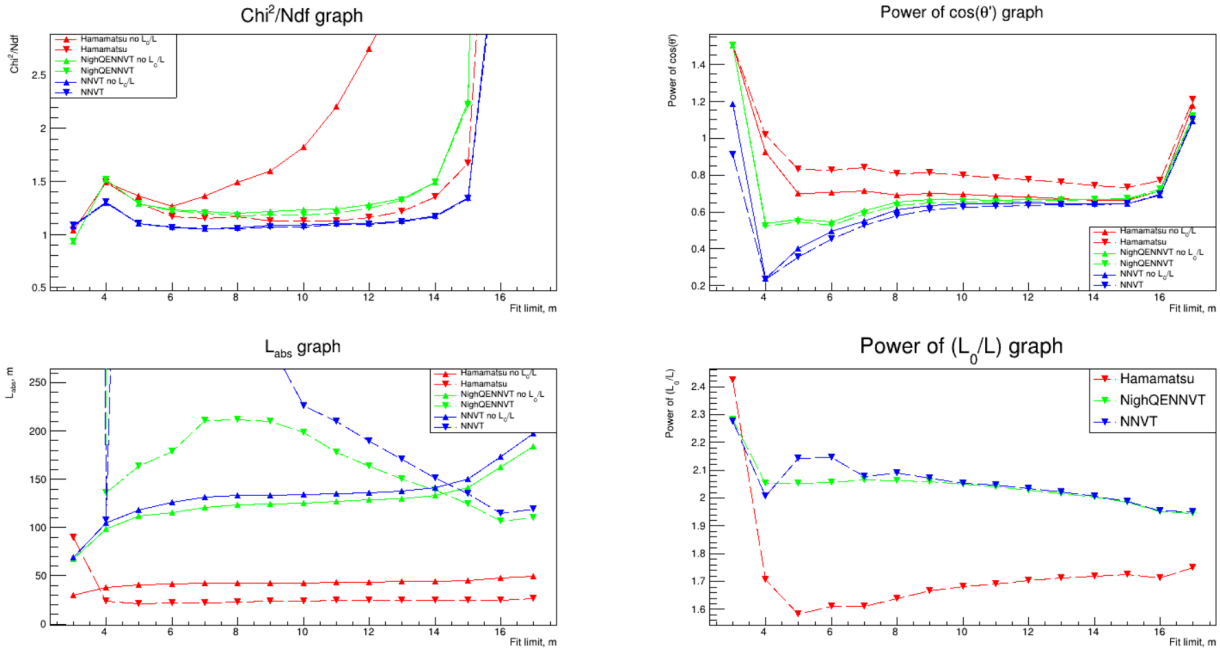

Fig. 2.5 — The results of the «N PMT» histogram fit by the analytical function (see Eq. 2.8) for each PMT type: Hamamatsu (red), HighQENNVT (green) and NNVT (blue). The graphs include the reduced χ^2 (upper right) and parameters of the fit: n (upper left), L_{att} (lower left) and m (lower right). If the parameter m of the fit is fixed at $m = 2$, the line is solid, if m is not fixed, then the line is dashed

For a more precise determination of L_{att} we studied the bins of the histograms that are close to the PMT axis of symmetry: $\cos\theta \approx \pm 1$, thus eliminating the angular dependency.

From the content of each of these bins, the D parameter (dark noise) was subtracted, and the content was multiplied by the distance L to the PMT squared (away with the $(\frac{L_0}{L})^2$ dependency). Finally, they were normalized by the value of the central bin (Fig. 2.6). The region of large distances between event and PMT (26 ÷ 33 m) was fitted with an exponential function (the results in tab. 2.1).

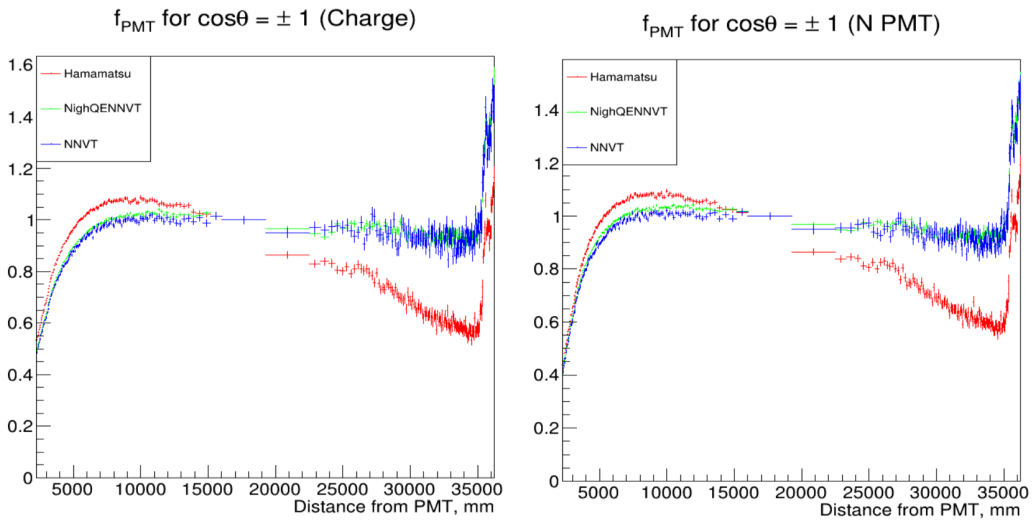

Fig. 2.6 — Bins of «Charge» and «N PMT» histograms corresponding to $\cos\theta = \pm 1$, with contents modified to extract pure exponential function $\exp(\frac{L-L_0}{L_{att}})$

Branch	L_{att} (m) by PMT type		
	Hamamatsu	HighQENNVT	NNVT
Charge	21.6±0.6	137.9±14.7	131.2±26.0
N PMT	22.9±0.6	131.5±11.2	117.1±17.3

Table 2.1 — The parameter L_{att} for different PMT types taken from the fit of «Charge» and «N PMT» histograms 2.5

3 CONCLUSION

In the present study

1) the coordinates of all 20-inch photomultiplier tubes of the JUNO detector were extracted, and their characteristics were evaluated;
2) a dataset of events was generated and analyzed using software developed by JUNO collaboration;
3) a comprehensive fitting procedure was employed to estimate the values of parameters in analytical approximation of the detector response;
4) a method for the fast event generation was studied and the basic groundwork was done for its implementation in JUNO.

However, issues with the evaluated parameters (attenuation length L_{att} in particular) remain: for two out of three PMT types the analysis yielded L_{att} values much greater than expected. The issue may lie in the present analysis (e.g. an error in the code) or in one of the steps of data generation.

ACKNOWLEDGMENTS

I thank JINR and the organizing committee of the START program for providing accommodation and paying for all needs during my stay in Dubna. Special thanks to Elena Karpova for helping resolve any arising problems and answering my incessant questions.

I am grateful to my supervisor Oleg Smirnov for his guidance and support throughout my time at Dzhelepov Laboratory of Nuclear Problems and the whole laboratory team for insightful conversations and help, which is much appreciated.

A TOTAL INTERNAL REFLECTION

In this appendix, we discuss the effect of total internal reflection (TIR) on the PMT light collection function.

Total internal reflection is the phenomenon of complete reflection of light at a boundary between media, if the refractive index n_1 of the first medium is larger than the refractive index n_2 of the second and the angle of incidence of the light ray is greater than the critical angle $\theta_c = \arcsin\frac{n_2}{n_1}$. It just so happens that such conditions can be satisfied in some events in the JUNO detector: the refractive indices are $n_{LS} = n_1 \approx \frac{3}{2}$ for the liquid scintillator in the CD and $n_{H_2O} = n_2 \approx \frac{4}{3}$ for the water in the WP.

First, let's find the distance from the center of the detector, at which the effect appears. The geometry of the problem is displayed below:

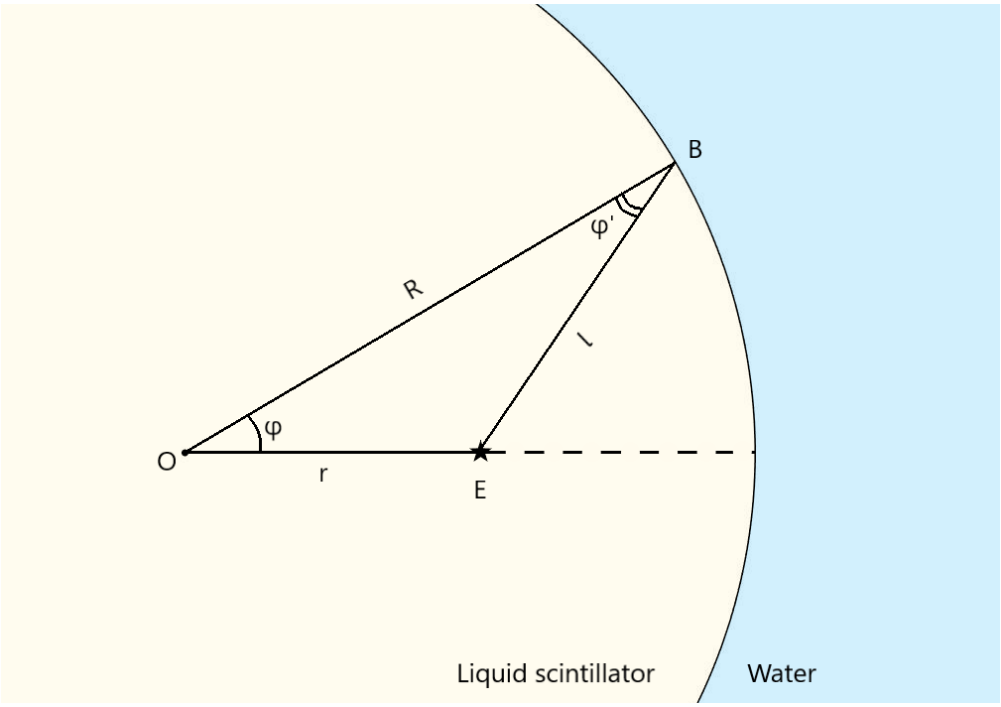

Fig. A.1 — Geometry of total internal reflection of scintillation light in a spherical detector

In Fig. A.1 O is the center of the detector, E is the event (scintillation) position, B is the border between liquid scintillator and water, R is the detector radius, r is the distance between the detector center and the event, φ' is the angle of incidence.

From Snell's law for total internal reflection, we get $\sin\varphi' = \frac{n_{H_2O}}{n_{LS}} = \sqrt{1-\cos^2\varphi'}$. Calculating the $\cos\varphi'$ from the cosine theorem, and solving the quadratic equation for $\cos\varphi$, we get

$$\cos\varphi_{\pm}(r) = \frac{R}{r}\left(\frac{n_{H2O}}{n_{LS}}\right)^2 \pm \sqrt{\left(1-\left(\frac{n_{H2O}}{n_{LS}}\right)^2\right)\cdot\left(1-\left(\frac{R}{r}\cdot\frac{n_{H2O}}{n_{LS}}\right)^2\right)} \tag{A.1}$$

Eq. A.1 gives for each event at the distance r from the center of the detector the borders of a «belt» on the surface of the detector, which will completely reflect the light back into the liquid scintillator. The minimal distance from the center r_{min}, where TIR of scintillation light is possible, corresponds to Eq. A.1 having a single solution. Thus, $r_{min} = R \cdot \frac{n_{H2O}}{n_{LS}}$, which for JUNO gives $r_{min} \approx 15.7$ m.

The LPMTs around the liquid scintillator, however, are mounted on the spherical stainless steel structure with a radius $L_0 = 19.4$ m. This means that the angles φ and θ (see Fig. 2.1) are not the equal, same for the angle of incidence φ' and polar angle θ' of the event in PMT frame of reference:

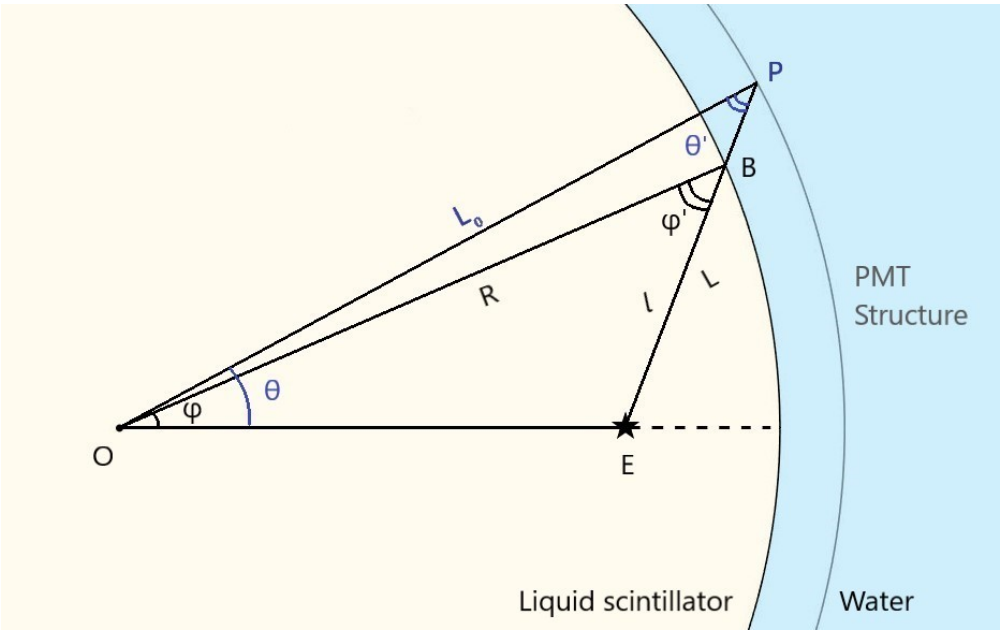

Fig. A.2 — Geometry of total internal reflection and PMT in a spherical liquid scintillator detector

Here P is the PMT position, θ, θ' and L bear the same meaning as in Fig. 2.1 and Eq. 2.1-2.3 (without the PMT numeration).

To find the relation between $\cos\theta$ and $\cos\varphi$, let us consider the ratio of areas of triangles ΔOBE and ΔOPE. On one hand, this ratio may be calculated as $\frac{l}{L}$, because the triangles share the same altitude. On the other hand, the areas can be computed using $\sin\theta$ and $\sin\varphi$. Substituting L and l for their expressions from the cosine theorem, we get

$$\frac{l}{L} = \frac{\sqrt{r^2+R^2-2rR\cos\varphi}}{\sqrt{r^2+L_0^2-2rL_0\cos\theta}} = \frac{\frac{1}{2}rR\sin\varphi}{\frac{1}{2}rL_0\sin\theta} \tag{A.2}$$

From Eq. A.2 a quadratic equation for $\cos\theta$ can be derived, the solution to which:

$$\cos\theta_{\pm}(r) = \frac{rL_0R^2\sin^2\varphi_{\pm}(r) \pm \sqrt{\frac{D_{\pm}(r)}{4}}}{L_0^2(r^2+R^2-2rR\cos\varphi_{\pm}(r))} \tag{A.3}$$

where

$$\frac{D_{\pm}(r)}{4} = r^2L_0^2R^4\sin^4\varphi_{\pm}(r) - L_0^2(r^2+R^2-2rR\cos\varphi_{\pm}(r))\times$$
$$\times\left(R^2\sin^2\varphi_{\pm}(r)(r^2+L_0^2) - L_0^2(r^2+R^2-2rR\cos\varphi_{\pm}(r))\right) \tag{A.4}$$

The solution A.3 gives the borders of a «blindness» belt: the PMTs cannot see events with coordinates r and $\cos\theta_-(r) < \cos\theta < \cos\theta_+(r)$. To use this solution in the fit of the margin region of histograms, we need a continuous function $F_M(r, \cos\theta)$, which would be an additional factor in Eq. 2.8 (multiplied only by the first term in f_{PMT}, because the dark noise constant is geometry-independent), equal to $F_M = 1$ in the central part of the detector volume and $F_M < 1$ in the margin region of interest. Usage of a sigmoid function was considered:

$$F_M(r,\cos\theta) = 2 - \frac{1}{1+\exp\left(-\frac{\cos\theta-\cos\theta_-(r)}{d}\right)} - \frac{1}{1+\exp\left(-\frac{\cos\theta_+(r)-\cos\theta}{d}\right)} \tag{A.5}$$

where d is an «abruptness» parameter, which measures the steepness of the curve and the size of the «transitional» region (if $d = 0$, the sigmoid function becomes a non-continuous step-function). Both the solution A.3 and the factor A.5 are displayed below:

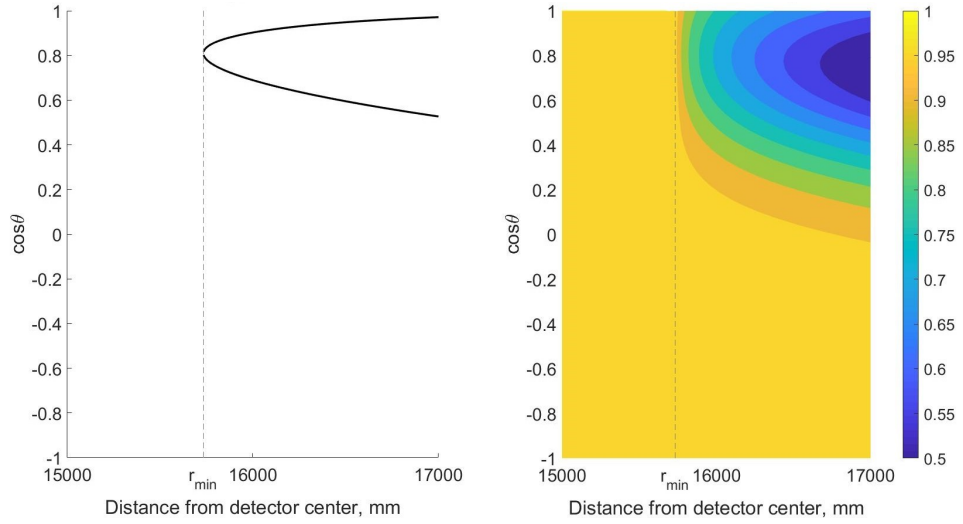

Fig. A.3 — Solution A.3, representing a «blindness» belt for the PMTs on the fitted histograms (left), and the factor F_M for the margin fit (right)

Unfortunately, the fitting was unsuccessful. Therefore, we leave the search for a suitable fitting function for future work.

BIBLIOGRAPHY

1. *JUNO collaboration.* JUNO physics and detector // Progress in Particle and Nuclear Physics. — 2022. — Vol. 123. — P. 103927. — ISSN 0146-6410.
2. Determination of the neutrino mass hierarchy at an intermediate baseline / L. Zhan [et al.] // Phys. Rev. D. — 2008. — Vol. 78, issue 11. — P. 111103.
3. Nuclear physics for geo-neutrino studies / G. Fiorentini [et al.] // Phys. Rev. C. — 2010. — Vol. 81, issue 3. — P. 034602.
4. New experimental limits on violations of the Pauli exclusion principle obtained with the Borexino Counting Test Facility / H. O. Back [et al.] // The European Physical Journal C - Particles and Fields. — 2004. — Vol. 37, no. 4. — P. 421–431. — ISSN 1434-6052.
5. *Смирнов О.* Habilitation thesis - Прямое измерение потока солнечных pp-нейтрино на детекторе Борексино. — URL: https://dissertations.jinr.ru/ru/Dissertations/Announcement/235.
6. Mass testing and characterization of 20-inch PMTs for JUNO / A. Abusleme [et al.] // The European Physical Journal C. — 2022. — Vol. 82, no. 12. — P. 1168. — ISSN 1434-6052.
7. Light attenuation length of high quality linear alkyl benzene as liquid scintillator solvent for the JUNO experiment / H. Yang [et al.] // Journal of Instrumentation. — 2017. — Vol. 12, no. 11. — T11004.
8. Refractive index in the JUNO liquid scintillator / H. S. Zhang [et al.]. — 2024. — arXiv: 2405.19879 [physics.ins-det].